



# Accelerator techniques and nuclear data needs for ion beam analysis of wall materials in controlled fusion devices

Marek Rubel<sup>1,2\*</sup> , Daniel Primetzhofner<sup>2</sup>, Per Petersson<sup>1</sup>, Sotirios Charisopoulos<sup>3</sup> and Anna Widdowson<sup>4</sup>

\*Correspondence: [rubel@kth.se](mailto:rubel@kth.se)

<sup>1</sup>Department of Plasma Physics, KTH Royal Institute of Technology, Stockholm, Sweden

<sup>2</sup>Department of Physics and Astronomy, Uppsala University, Uppsala, Sweden

Full list of author information is available at the end of the article

## Abstract

A brief overview of ion beam analysis methods and procedures in studies of materials exposed to fusion plasmas in controlled fusion devices with magnetic confinement is presented. The role of accelerator techniques in the examination and testing of materials for fusion applications is emphasised. Quantitative results are based on robust nuclear data sets, i.e. stopping powers and reaction cross-sections. Therefore, the work has three major strands: (i) assessment of fuel inventory and modification of wall materials by erosion and deposition processes; (ii) equipment development to perform cutting-edge research; (iii) determination of nuclear data for selected ion-target combinations. Advantages and limitations of methods are addressed. A note is also given on research facilities with capabilities of handling radioactive and beryllium-contaminated materials.

## 1 Introduction

Energy research driven by the quest for effective sources and means of electricity production is crucial for sustainable development. Despite distinct progress in energy-saving technologies and increasing number of installations based on fossil-free sources, the demand for electricity generation is ever growing to ensure functioning of transport, lighting, tele-communication and all branches of industry which require stable and high power supply. Simultaneously strong emphasis is on the safe and environmentally sound means of energy generation, while the production volume may be limited by the access to natural resources, currently available technologies, climate, and also by political situation.

Development of future technologies like Generation IV nuclear reactors and controlled thermonuclear fusion has a long history. In both cases, integrated efforts in science and technology are directed towards the construction and operation of reactor-class facilities. Controlled fusion is a multidisciplinary field encompassing plasma and ion physics, remote handling (RH) and radiofrequency (RF) technologies, nuclear physics and chemistry, demanding civil engineering, radiation protection and countless aspects of materials science and engineering. The latter extends from the composition and structure of concrete for a base of a reactor containment to the detailed characterisation of the plasma-facing

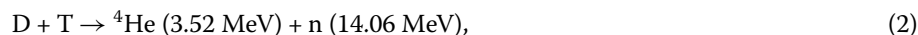
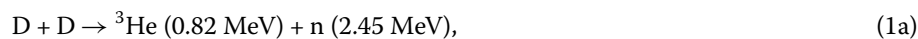
© The Author(s) 2023. **Open Access** This article is licensed under a Creative Commons Attribution 4.0 International License, which permits use, sharing, adaptation, distribution and reproduction in any medium or format, as long as you give appropriate credit to the original author(s) and the source, provide a link to the Creative Commons licence, and indicate if changes were made. The images or other third party material in this article are included in the article's Creative Commons licence, unless indicated otherwise in a credit line to the material. If material is not included in the article's Creative Commons licence and your intended use is not permitted by statutory regulation or exceeds the permitted use, you will need to obtain permission directly from the copyright holder. To view a copy of this licence, visit <http://creativecommons.org/licenses/by/4.0/>.

wall, i.e. plasma-facing materials (PFM) and components (PFC); both abbreviated jointly in the following as PFMC. The surface state of the latter class of materials is studied mainly by accelerator-based methods commonly called ion beam analysis (IBA).

In the interdisciplinary field of fusion research, the role of particle accelerators is at least five-fold: (i) ion beam analysis (IBA) of materials retrieved from vacuum vessels of controlled fusion devices; (ii) ion-induced simulation of neutron radiation effects in surfaces of solids; (iii) provision of nuclear data for ion-material interactions; (iv) ion-induced neutron generation for the material irradiation facility; (v) high current units in the neutral beam injection system for plasma (deuterium and tritium: D and T) heating. The first three aspects will be presented in the following sections with a focus on the role of accelerator techniques in the examination and testing of materials for fusion applications. Quantitative results can only be obtained using highly advanced laboratory equipment and combined with robust sets of nuclear data, i.e. stopping powers and reaction cross-sections. Therefore, the work has three essential strands: (a) assessment of fuel inventory and modification of PFMC composition by erosion and deposition processes; (b) equipment development to perform cutting-edge research; (c) determination of nuclear data for selected ion-target combinations.

## 2 Controlled fusion and plasma-wall interactions: impact on materials

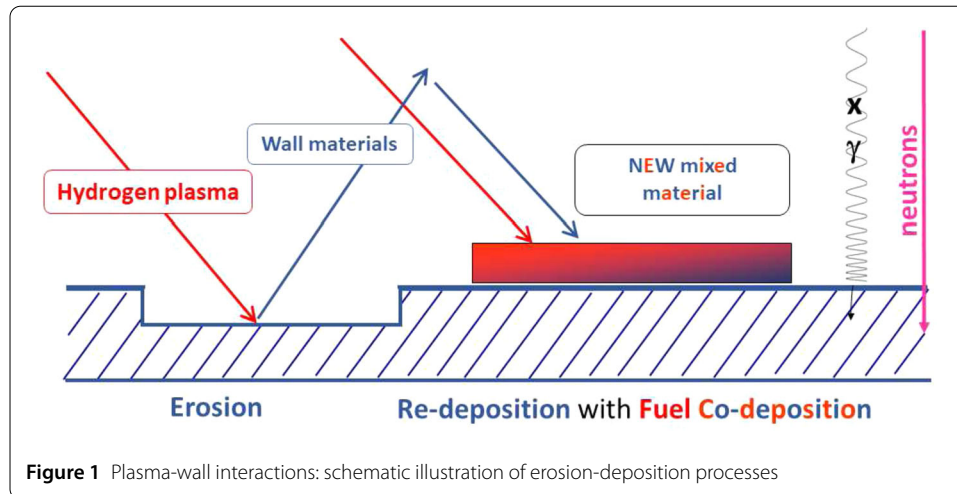
The goal of controlled thermonuclear fusion is to harness energy that powers stars: reactions of light nuclei characterised by  $Q$  values of several MeV and high reaction rates:



the branching ratio of Reactions (1a) and (1a) is around one. Deuterium fuel is used in most present-day devices, but the  $Q$  value (17.58 MeV) and the cross-section of the DT process [1, 2], favours that mix of hydrogen isotopes as a fuel for a reactor in a future power station. Reaction (3) has a significantly lower cross-section than Reaction (2) and, currently cannot be considered because of a very limited availability of  ${}^3\text{He}$ .

Two major schemes of fusing nuclei have been developed. Inertial confinement fusion (ICF) uses high power photon (laser) [3] or ion beams [4] focused on a small ( $\sim 1$  mm in diameter) D-T containing pellet placed in a vacuum chamber of a few meters in diameter. Magnetic confinement fusion (MCF) is based on plasmas generated and maintained by magnetic fields of a few T in toroidal systems [1, 5]. The latter scheme exploits two reactor concepts: tokamaks [1, 6] and stellarators [7]. In either case, both ICF and MCF, under terrestrial conditions the fusion plasma must be surrounded by walls of a vacuum vessel and, the energy released must then be absorbed by wall structures: 20% related to  ${}^4\text{He}$  ( $\alpha$  particles) by PFMC [8], while the neutron energy (80% of the total) is to be transferred to a  ${}^6\text{Li}$ -enriched blanket where the conversion to heat and tritium production will occur [9, 10].

The energy confinement time ( $\tau_E$ ) of particles of up to 1.0-1.5 s is shorter than the plasma discharge time. Consequently, particles escape the plasma and impinge on the wall. These



are electrons, ions at different ionisation states and charge exchange neutrals (CXN). In addition, there are neutrons generated in fusion reactions as well as electromagnetic radiation with a broad energy spectrum from RF down to hard gamma and X-rays. They are decisive for what is called plasma-wall interactions (PWI) which involve a huge range of processes: physical sputtering, chemical erosion, reflection, implantation, gas retention, desorption, melting, boiling, splashing, arcing, cracking, ionisation, recombination, compound formation, activation and consequential transmutation [8, 11–13]. All of them are dynamic arising from atomic, molecular and nuclear physics and chemistry.

A scheme of interactions is shown in Fig. 1. Eroded species are immediately ionised and travel along the magnetic field lines. Eventually, if not pumped out, the migrating species are re-deposited in a close or distant location with respect to the place of origin. Re-deposition involves atoms of different elements originally eroded from the wall. It is a simultaneous co-deposition in which also fuel atoms are included. As a result, mixed material layers are formed. The composition and other properties of such deposition zones significantly differ from those of the original substrates. Thermo-mechanical incompatibility between the substrate and co-deposit may lead to flaking and spalling-off of the layer thus forming dust which constitute a major operational issue if large amounts of dust are formed and, if such particles contain considerable fraction (a few atomic %) of fuel atoms, especially radioactive tritium or neutron-activation products.

In short, PWI comprises all processes of energy and mass exchange between the plasma and the surrounding surfaces. As a result, the plasma and the wall are modified with serious consequences for reactor operation. The plasma gets contaminated and loses energy, while properties of PFMC and some crucial tools for plasma diagnosis (mirrors and windows) are changed. This has an impact on the material lifetime and fuel inventory thus for the reactor safety. PWI processes are both unavoidable and necessary. The wall provides vacuum conditions indispensable for operation, removes heat and - only under DT reactor conditions - ensures final thermalization of helium ash to enable its pump out, and absorption of energetic neutrons in the blanket for tritium productions and power generation.

In-vessel materials must be, in the first place, compatible with vacuum and strong magnetic fields, while the list of requirements for PFC candidates comprises in addition: high

thermal conductivity ( $\lambda$ ), i.e. over  $150 \text{ W m}^{-1} \text{ K}^{-1}$ , resilience to thermal shocks, low erosion yield by plasma species, low sorption of hydrogen isotopes to limit fuel inventory, high melting ( $T_m$ ) and boiling ( $T_b$ ) points, low-Z to minimise plasma energy losses by impurities, low erosion rate, low affinity to fuel and to oxygen impurities towards the formation of volatile products, affinity to oxygen impurities towards their gettering to form solid oxides, low neutron-induced activation. None of the known substances can fulfil such requirements, especially that some of them are contradictory. Therefore, the material selection is based on the approach that properties should change as little as possible under plasma impact.

The major materials of interest for PFC are beryllium (Be), carbon (C) in the form graphite or carbon fibre composites (CFC), and tungsten (W). In addition, molybdenum (Mo) is important as material for so-called first mirrors, i.e. plasma-facing materials in optical diagnostics. Crucial advantages and drawbacks of respective wall materials are compiled in Table 1, while very detailed characteristic can be found in [8]. Graphite and several types of CFC have been used in toroidal devices since seventies of the 20th century because of their excellent power handling capabilities. Issues related to the erosion rates and the formation of fuel-rich co-deposits were known, but their dramatic seriousness was recognised after full D-T campaigns in TFTR [14, 15] and JET [16–21] operated with carbon walls: nearly 30% of the injected tritium was retained in the vessel, especially in the remote areas of the divertor, i.e. places shadowed from the direct plasma line-of-sight. Such locations are very difficult to reach by any cleaning method [18, 20, 22]. No efficient means of fuel removal have been developed and the use of carbon in a D-T fusion reactor had to be reconsidered [22–27]. A large scale-test with all-metal walls was decided at the largest tokamak in the world: the Joint European Torus (JET) [28–30]. Carbon PFC were removed and replaced by solid Be limiters and Be coatings on the main chamber wall [31, 32], while W components (bulk metal and coatings on CFC tiles) were installed in the divertor [32–34]. The operation of JET with the ITER-like wall (JET-ILW) started in 2011 and, it was clearly shown that the elimination of carbon sources resulted in a significant decrease of fuel retention [35–42] and dust generation [43–48]. In a consequence, the ITER Organisation decided to abandon carbon components in the divertor and prepare for operation with Be panels in the main chamber and tungsten in the divertor [49].

**Table 1** Key properties of C and metals as wall materials and diagnostic components

Element	Advantages	Drawbacks/Limitations	Remarks
C	Low-Z. Resilience to thermal shocks and no melting $\lambda$ of some CFC $> 300 \text{ W m}^{-1} \text{ K}^{-1}$ .	Chemical erosion by fuel atoms, $\text{C}_x\text{H}_y$ formation, high erosion rate and fuel inventory in co-deposits.	PFMC in most tokamaks [8, 14–21, 27, 50–55] and stellarators [56–58] because of excellent power handling capabilities.
Be	Low-Z, no chemical erosion	Low $T_m$ and high sputter yield.	Used in JET-ILW in the main chamber wall [29, 31, 59]; the same decided for ITER wall [49].
W	High $T_m$ and low sputter yield by fuel	High-Z, risk for plasma contamination and disruptions. Activation and transmutation.	ASDEX Upgrade wall and divertor [60, 61]. JET-ILW divertor [29, 32–34, 62]; the same decided for ITER divertor [49].
Mo	High $T_m$ and low sputter yield by CXN	High activation.	Tested candidate for first mirrors in ITER diagnostic systems [63–67]

The major research objectives are to determine: (i) the lifetime of PFMC; (ii) in-vessel fuel accumulation, i.e. to obtain quantitative mapping of the distribution of D and T; (iii) quantity and properties of dust with particular emphasis on the identification of sources, generation pathways and fuel content; (iv) plasma impact on diagnostic components which are crucial for plasma characterisation and machine protection. All of them are decisive for reactor economy and safety. As such, these are key points in the licensing process. *Conditio sine qua non* for conclusive studies is the access to materials (specimens from diverse locations: wall tiles, probes, dust) retrieved from the vacuum vessel after experimental campaigns. Research requires a huge variety of material characterisation methods. It directly implies the access to laboratories with relevant apparatus, competent research teams and – in many cases – capabilities and certificates for handling radioactive materials: T-contaminated and activated.

### 3 Analysis methods and instrumentation

#### 3.1 Analysis: needs and methods

Over the years, more than fifty different material characterisation techniques have been used in the PFMC research: ion, electron, neutron and optical spectroscopies, methods based on probing solids with magnetic field, sound waves, mechanical force or thermal means applying either a steady temperature rise or shocks by flash heating. The variety of probing ('signal in') and detection means ('signal out'), their broad energy spectrum and a range of physical processes involved in the interactions create a huge number of "signal in – signal out" combinations, and – by this – research opportunities. Nearly every combination may actually be applied in a certain area of material characterization. However, only most efficient, methods for analyses of PFMC are mentioned in the following, i.e. techniques capable of sensitive and selective quantitative determination of the content and distribution (in-depth and lateral) of a wide range of elements and, in many cases, their particular isotopes present in the examined materials. Capabilities for mapping surface species on large areas on the tiles (e.g.  $15 \times 20$  cm) are also required in many cases. Compositional analyses must cover a broad range of species which are present in the wall and diagnostic components, fusion fuel and gases injected for auxiliary plasma heating, plasma edge cooling, disruption mitigation, wall conditioning, or as markers (tracers) in material migration studies. As a result, the list extends from H, D, T,  $^3\text{He}$ ,  $^4\text{He}$  and other noble gases (Ne – Xe), isotopes of Li, Be, B, C, N, O, F to heavier species such as Al, Si to Cr, Fe, Ni and then to W, Re; even Au is to be taken into account. The role and origin of respective species in the reactor is addressed in Table 2 in which also the information on relevant analysis methods is conveyed.

The requirement for lateral mapping and depth profiling of such diverse compositions are met by IBA methods. Their detailed description with the underlying physics basis can be found in [68, 69], while the role in PFMC analysis has been addressed in overview articles [70–72]. IBA is based on the irradiation of a solid target with an ion beam followed by a detection and analysis of energy and/or mass spectra of signals emitted from the surface: reflected primary ions, products of nuclear reactions, recoiled atoms, photons (from visible to X and gamma rays), sputtered species such as secondary ions (monoatomic and molecular) and neutrals. Dependent on the ion (type, energy) – signal combination there is a number of methods governed by different physical processes.

- Rutherford Backscattering Spectrometry (RBS) mainly with  $^4\text{He}^+$  in the 1.5 – 3 MeV energy range.

**Table 2** Species to be analysed/determined and their role in a reactor

Species	Origin and role in a reactor	IBA Method	Reaction (of practical use)*	Remarks and references
H	Wall cleaning - conditioning gas	NRA, ERDA	$^1\text{H}(^{15}\text{N},^4\text{He})^{12}\text{C}$	H is always present in vacuum systems; information depth below 1 $\mu\text{m}$ ; strong detrapping by the $^{15}\text{N}$ beam.
D	Fuel	NRA, ERDA, EPS	$^2\text{D}(^3\text{He},^1\text{H})^4\text{He}$	NRA is the main technique in D analysis [70–80]. Depth profiling in C-H layers to over 30 $\mu\text{m}$ at 6 MeV [73]
T	Fuel	NRA, ERDA, AMS	$^3\text{T}(^{12}\text{C},^4\text{He})^{11}\text{B}$ $^3\text{T}(^{12}\text{C},^1\text{H})^{14}\text{C}$ $^3\text{T}(^4\text{He},\text{n})$	Use of IBA is limited. Low sensitivity of $^{12}\text{C}-^3\text{T}$ reactions $^{12}\text{C}-^3\text{T}$ reactions tried on JET materials [81], while the $^2\text{D}-^3\text{T}$ was used on TFTR tiles [82]. AMS in trace analysis [83].
$^3\text{He}$	Minority gas for ICRF heating	ERDA		[84]
$^4\text{He}$	Ash of D-T reaction; Wall cleaning - conditioning gas	ERDA		[84]
$^6\text{Li}$ ; $^7\text{Li}$	Li-beam diagnostic, wall coatings	NRA, ERDA, PIGE	$^7\text{Li}(^1\text{H},\text{n}\gamma)^8\text{Be}$	
$^9\text{Be}$	Wall material	NRA, ERDA	$^9\text{Be}(^3\text{He},^1\text{H})^{11}\text{B}$ $^9\text{Be}(^2\text{D},^1\text{H})^{10}\text{Be}$ $^9\text{Be}(^2\text{D},^4\text{He})^7\text{Li}$	[20, 71, 72, 75, 77, 85]
$^{10}\text{Be}$	Be migration marker	AMS		Marker n-activated $^9\text{Be}$ tile [86]
$^{10}\text{B}$ and $^{11}\text{B}$	Wall conditioning by low plasma in $\text{B}_2\text{H}_6$ , $\text{B}(\text{CH}_3)_3$ or evaporation from $\text{B}_{10}\text{H}_{14}$	NRA, ERDA	$^{11}\text{B}(^1\text{H},^4\text{He})^8\text{Be}$ $^{11}\text{B}(^3\text{He},^1\text{H})^{13}\text{C}$	Analysis of PFMC from boronised machines [87–91]
$^{12}\text{C}$	Wall material	NRA, EPS, ERDA	$^{12}\text{C}(^3\text{He},^1\text{H})^{14}\text{N}$ $^{12}\text{C}(^2\text{D},^1\text{H})^{13}\text{C}$ $^{12}\text{C}(^1\text{H},^1\text{H})^{12}\text{C}$	[18, 70–72, 77, 78, 92] $^{12}\text{C}(^2\text{D},^1\text{H})^{13}\text{C}$ for C analysis on Be targets [85]
$^{13}\text{C}$	Tracer in C migration studies	NRA, EPS, ERDA	$^{13}\text{C}(^3\text{He},^1\text{H})^{15}\text{N}$ $^{13}\text{C}(^1\text{H},^1\text{H})^{13}\text{C}$	[93–96]
$^{14}\text{N}$	Edge cooling	NRA, ERDA	$^{14}\text{N}(^2\text{D},^1\text{H})^{15}\text{N}$ $^{14}\text{N}(^2\text{D},^4\text{He})^{12}\text{C}$	[85, 93, 97, 98]
$^{15}\text{N}$	Tracer	NRA, ERDA	$^{15}\text{N}(^1\text{H},^4\text{He}\ \gamma)^{12}\text{C}$	[96, 98]
$^{16}\text{O}$	Major impurity	RBS, EPS, NRA, ERDA	$^{16}\text{O}(^2\text{D},^1\text{H})^{17}\text{O}$ $^{16}\text{O}(^1\text{H},^1\text{H})^{16}\text{O}$	[93]
$^{18}\text{O}$	Tracer for in-vessel oxidation studies	NRA, ERDA	$^{18}\text{O}(^1\text{H},^4\text{He})^{15}\text{N}$	[65, 78]
$^{20}\text{Ne}$	Edge cooling agent	ERDA, RBS		[84, 97]
$^{21}\text{Ne}$ , $^{22}\text{Ne}$	Considered as tracers	ERDA, RBS		RBS only on light substrates
Al	Impurity from structural material of RH systems	RBS, PIXE, ERDA		
Si	Component of in-vessel diagnostics	RBS, PIXE, ERDA		$\text{SiH}_4$ ( $\text{SiD}_4$ ) used for wall conditioning (siliconisation) [99]

**Table 2** (Continued)

Species	Origin and role in a reactor	IBA Method	Reaction (of practical use)*	Remarks and references
Ar	Edge cooling agent	RBS, PIXE, ERDA		[94]
Fe, Cr, Ni	Vacuum vessel and antennae materials: Steel, Inconel	RBS, PIXE, ERDA, MEIS		Separation with RBS is difficult. ERDA and particularly MEIS allow separation of Cr and Ni [100]
Cu	Impurity from NBI system	RBS, PIXE, ERDA		PIXE in presence of Fe, Cr, Ni
Kr	Edge cooling agent	RBS, PIXE, ERDA		[94]
Mo	Vacuum vessel and antennae materials: Steel, Inconel; First mirrors	RBS, PIXE, ERDA		
W	Wall material	RBS, PIXE, ERDA, MEIS		MEIS: [100, 101]
Re	Proposed addition to W	RBS, PIXE, ERDA		Only PIXE in the presence of W
Au	In-vessel diagnostics: bolometers, coated mirrors	RBS, PIXE, ERDA		

\* Only reactions of practical use are listed, i.e. reactions with the detection limit of minimum  $5 \times 10^{14} \text{ cm}^{-2}$ .

- Elastic Backscattering Spectroscopy (EBS) employing enhanced cross-sections for scattering of  $^4\text{He}^+$  from C and O in the energy range 3-5 MeV.
- Non-Rutherford Enhanced Proton Scattering (EPS) with  $\text{H}^+$  in the 0.5 – 2.5 MeV range.
- Nuclear Reaction Analysis (NRA) – a huge variety of analytical capabilities using low-Z ion beams: mainly  $^3\text{He}^+$  (0.6 – 6 MeV) and  $\text{H}^+$ , but also  $\text{D}^+$ ,  $^{12}\text{C}$ ,  $^{15}\text{N}$  and  $^{16}\text{O}$  ions. Respective nuclear reactions are in Table 2.
- Particle Induced X-ray Emission (PIXE) and/or Gamma Emission (PIGE) using a primary 1.5 – 4 MeV beams of  $\text{H}^+$ ,  $^3\text{He}^+$ ,  $^4\text{He}^+$ .
- Time-of-Flight Elastic Recoil Detection Analysis (ToF-ERDA) with  $^4\text{He}^+$  or the high ion version (ToF- HIERDA) using for instance multiply charged ion beams of  $\text{C}^{n+}$ ,  $\text{Si}^{n+}$ ,  $\text{Br}^{n+}$  or  $\text{I}^{n+}$  beams. Depth profiling extends from 300 nm in heavy metal targets up to 800 nm in low-Z materials.
- Accelerator Mass Spectrometry (AMS) in trace analysis of T,  $^{10}\text{B}$ ,  $^{14}\text{C}$ .
- Medium Energy Ion Scattering (MEIS) using a 50 – 400 keV  $^4\text{He}^+$  beam.
- Secondary Ion Mass Spectrometry (SIMS) with primary beams of  $\text{Ar}^+$ ,  $\text{Cs}^+$  or  $\text{O}^-$  of a few keV. The method is sensitive but its use is limited because the quantification in complex mixed-material co-deposits is difficult.

For most techniques, besides ERDA, the standard lateral resolution determined by beam diameter is in the range 0.6-1.2 mm. Detailed mapping of species with a resolution of 1-30  $\mu\text{m}$  is carried out (if needed) with  $\mu$ -RBS,  $\mu$ -NRA,  $\mu$ -EPS and  $\mu$ -PIXE, i.e. using micro-beams formed in a quadrupole-equipped beamline. In ERDA or HIERDA which are



based on the target irradiation at a shallow angle (usually  $22.5^\circ$ ) the beam spot is elongated:  $1 \times 4$  mm.

Taking into account a range of ion beams, beam spot size, broad energy spectrum, tens of nuclear reactions and data processing software, the “toolbox” offers a huge number of analytical options. It is also clear that there is no single technique to address all needs taking into account the differences in the information depth and sensitivity for detecting respective species because these parameters are decided by energy-dependent stopping powers in ion-target systems, and by cross-sections of individual processes.

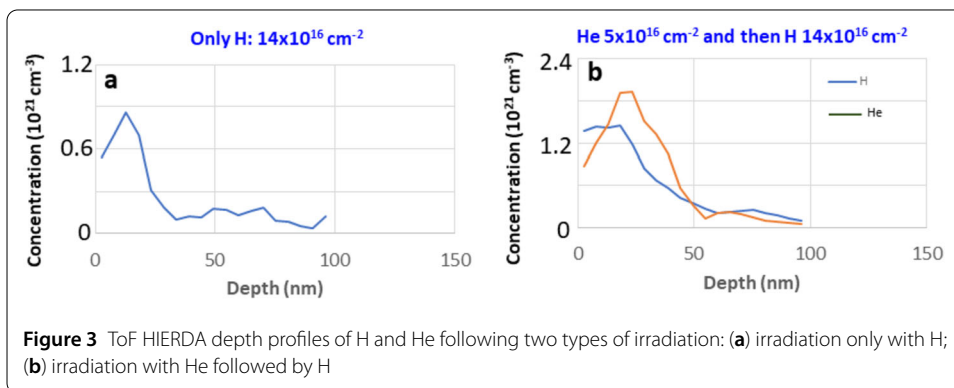
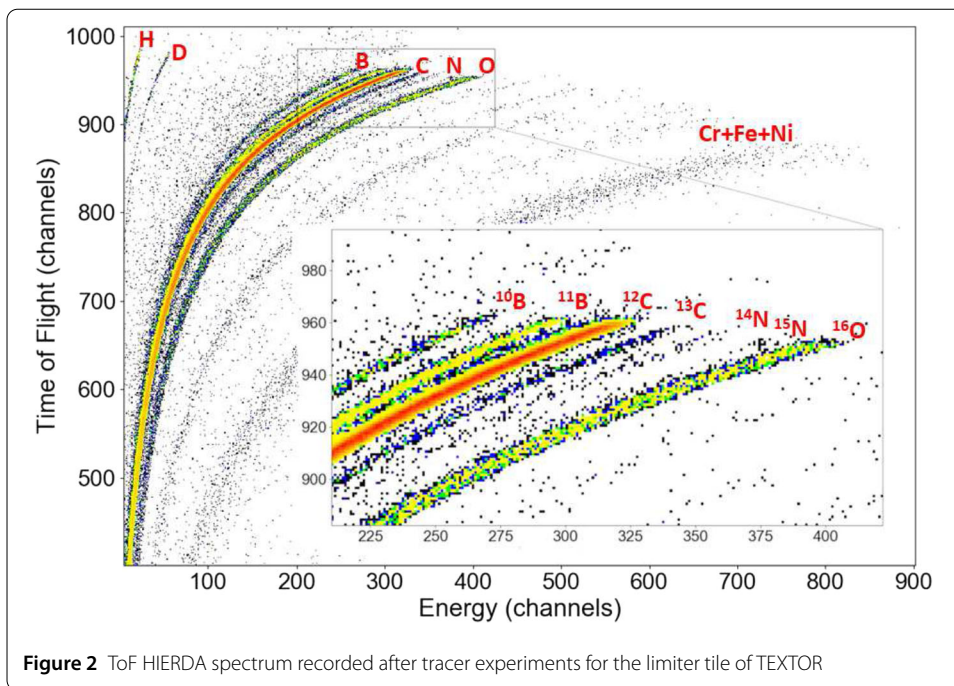
The IBA methods are complementary to each other and, they are complementary to other techniques for the characterisation of PFMC and fuel inventory. In the case of light isotopes, particularly in fuel retention studies,  $^3\text{He}$ -based NRA plays a prominent role. It is the only method to determine quantitatively the areal distribution and depth profiles of deuterium down to tens of micrometres in light substrates [73]. Micro-NRA facilities deuterium mapping in regions with a highly not uniform content of that isotope [102] and, even in single grains of dust [74, 103–105]. NRA complements results of the gas balance assessment in fusion devices [50, 79, 106, 107] and thermal desorption spectroscopy (TDS) data [108] to obtain an overview of the global fuel retention. Determination of the fuel content in PFMC is crucial to obtain reference targets in the development of in-situ techniques: laser-induced desorption (LIDS), breakdown (LIBS) or ablation (LIAS) spectroscopy techniques [109–114].

In the third column of Table 2 ERDA is listed in every set of useful/recommended techniques. ToF-HIERDA is an extremely powerful tool in the determination of low-Z isotopes on surfaces, especially when using a gas ionization chamber (GIC) detector [115], as it has been shown in studies of PFMC and wall probes from the TEXTOR [89, 90], JET [77], COMPASS [91] tokamaks, and from laboratory experiments on mirror testing [116]. A great advantage is a simultaneous analysis of H, D,  $^3\text{He}$  and  $^4\text{He}$  [84]. High mass resolution facilitates conclusive results in material migration studies which involve the injection of tracer gases labelled with rare isotopes such as  $^{13}\text{CH}_4$  [90],  $^{15}\text{N}_2$  [90],  $^{18}\text{O}_2$  [65, 84] when it is essential to discriminate between the main and minor isotopes, e.g.  $^{12}\text{C}$  eroded from PFMC and the injected  $^{13}\text{C}$  tracer. The GIC detector opens possibilities for applying other tracers:  $^{10}\text{B}_2\text{H}_6$ ,  $^{21}\text{Ne}$ ,  $^{22}\text{Ne}$ . Figure 2 shows a spectrum recorded with a 42 MeV  $^{127}\text{I}^{8+}$  beam on the PFC surface retrieved from the TEXTOR tokamak after experiments with  $^{13}\text{CH}_4$  and  $^{15}\text{N}_2$  tracers.

### 3.2 Ion-induced damage in materials

The other role of accelerators in fusion research is in the ion-induced simulation of neutron damage in materials [10, 116–118]. The damaged surface structure has a major impact on fuel retention in PFC and, also on optical performance of crucial diagnostic components like so-called first mirrors, i.e. metal mirrors acting as plasma-facing components in all optical plasma diagnosis systems (spectroscopy and imaging) in ITER, i.e. the reactor-class machine under construction. The impact of irradiation with H,  $^4\text{He}$  (transmutation simulation) and Mo, Zr, Nb (simulation of n-induced damage) on the optically active layer of Mo mirrors has been presented [116, 117]. There are three key points in such study: (i) the selection of irradiation conditions by H,  $^4\text{He}$  and high-Z species to influence changes in the optically active layer (OAL) of the mirror, i.e. maximum 20 nm of the outermost surface; (ii) the irradiation and determination of reflectivity changes; (iii)





ToF HIERDA measurements of H and <sup>4</sup>He depth profiles, their changes in time, and the dependence on the irradiation sequence. Plots in Fig. 3(a) and (b) show, respectively, depth profiles of H and He following the irradiation of polycrystalline Mo mirrors only with a 2 keV H<sup>+</sup> beam  $14 \times 10^{16} \text{ cm}^{-2}$  and, first with  $5 \times 10^{16} \text{ cm}^{-2}$  of 2 keV <sup>4</sup>He<sup>+</sup> and then with  $14 \times 10^{16} \text{ cm}^{-2}$  of 2 keV H<sup>+</sup>. The results indicate that the damage produced by He has a strong impact on the amount and depth distribution of hydrogen: the H profile is deeper when combined with the implantation of He. Secondly, the H retention is doubled after the He<sup>+</sup> irradiation in comparison to the irradiation with H<sup>+</sup> only: from 2% to 4% atomic.

### 3.3 Instrumentation

A pre-requisite for the advanced accelerator-based material research, either analysis or modification, is a laboratory (or a network of laboratories) with equipment providing a broad range of capabilities regarding the beam composition, energy, current, particle detection and, the control of experimental parameters: gas feed, temperature etc. An overview of accelerator laboratories with a detailed account on the facilities relevant to

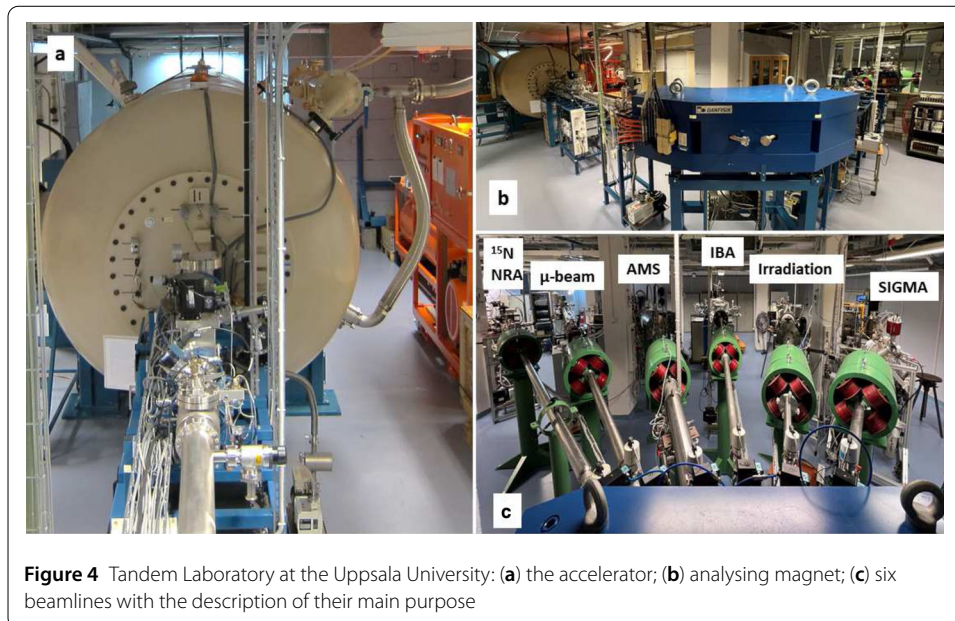


**Figure 4** Tandem Laboratory at the Uppsala University: (a) the accelerator; (b) analysing magnet; (c) six beamlines with the description of their main purpose

studies of fusion-related materials has been given in [72]. Among them, there are six laboratories capable of handling and analysing Be- and T- contaminated materials from JET: from full not sectioned Be tiles (12 cm × 20 cm) to smaller samples, and even to individual dust particles. Work procedures with such materials (handling, transport etc.) have been addressed in [71, 72], while very details are in [119].

New developments of the instrumentation are crucial to enhance and to broaden research capabilities. Images in Fig. 4 show the 5 MV pelletron tandem (National Electrostatic Corporation, NEC) and the beamline arrangement at the Tandem Laboratory, Uppsala University, Sweden. Two gas and two sputter ion sources allow for the formation of beams in all mass ranges, from low-Z (H - Li), medium-Z (Be - Si) and, with some exceptions, high-Z up to Au. There are six beamlines for standard IBA (PIXE, RBS, NRA and ToF ERDA with GIC detector [115]) and very specific tasks like <sup>15</sup>N NRA with a gamma detector, AMS used mainly in the <sup>10</sup>Be [86] and <sup>14</sup>C analyses, μ-beam with PIXE, RBS, NRA. A separate line is dedicated to material modification by ion irradiation, while the newly developed system on the sixth beamline is for in-situ and in-operando research: Set-up for *In-situ* Growth, Material modification and Analysis (SIGMA) [120, 121].

As already mentioned, all processes involved in PWI are dynamic. Direct in-situ material studies inside fusion devices are technically either very challenging or not possible at all. Some fundamental processes can therefore be investigated under controlled laboratory conditions. The SIGMA system, presented in Fig. 5(a) and (b), has been designed to facilitate material modification with in-situ IBA employing both light and heavy beams for RBS, EPS, EBS, NRA, PIXE, PIGE, ToF-ERDA at the 2- 50 MeV energy range. Due to large viewing ports optical characterization is also carried out. Several gas feeds, three evaporation cells, a sputter gun (1-5 MeV) enable diverse material modification scenarios. Sample annealing to 1100°C combined with gas phase analysis offers a wide range of experimental possibilities in studies of fuel retention in fusion-relevant targets.

Two other accelerating systems at Uppsala University further extend research on material modification [121]. With a 350 kV implanter (Danfysik) equipped with three change-

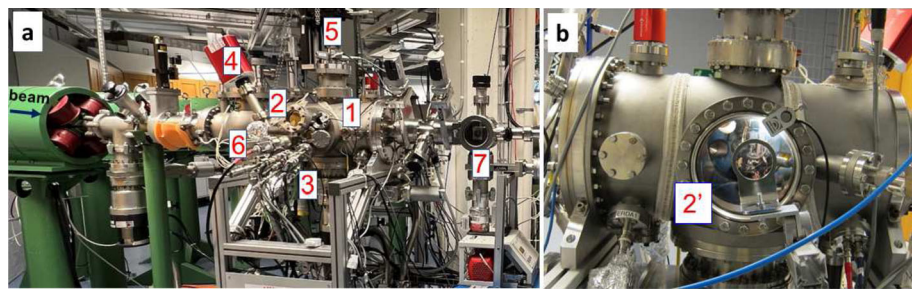


**Figure 5** SIGMA system shown from the both sides (a) and (b) of the apparatus: the vacuum chamber – 1; viewing ports on both sides of the chamber – 2 and 2'; triple evaporator – 3; residual gas analyzer – 4; sample manipulator – 5; ion gun – 6; load-lock chamber – 7

able ion sources (gas, oven-based, sputter) the simulation of neutron-induced damage by means of light and heavy ion irradiation is carried on mirrors tested for diagnostic and heating systems in future fusion devices [116–118]. Two other beamlines are for: (i) ToF-MEIS and (ii) low energy RBS and NRA. The application of MEIS [100, 101] ensured sensitive high resolution determination of surface composition and, has led to new topics in material modification and migration studies.

A low energy ion gun (up to 10 kV) in another system equipped with two chambers is the base for ToF Low Energy Ion Scattering (ToF LEIS), Auger Electron Spectroscopy (AES) and Low Energy Electron Diffraction (LEED) [122]. Material modification capabilities annealing, sputtering and in-situ growth of thin layers. In all materials analyses, the quantification of composition is essential. In the case of IBA, it relies on the energy dependent cross-sections in the interactions of fast particles with matter.

#### 4 Stopping and reaction cross-sections

The energy deposition by energetic charged particles in matter is conveniently described by the energy deposition per unit path length, commonly referred to as stopping power (S). Dependent on the nature of the interaction, i.e. whether energy is deposited by elastic interaction between ion and target nuclei or by excitation of the electronic system of the target, one refers respectively to electronic ( $S_e$ ) or nuclear ( $S_n$ ) stopping power [123]. By a convenient transformation one obtains the stopping cross section by normalization by the atomic density N, which yields a quantity independent of the mass density of the target material. In any representation, accurate knowledge on the specific energy deposition of charged particles forms a key ingredient for quantification in ion beam analytical methods, by providing depth scales, in ion implantation by allowing for a prediction of particle range and in modelling of e.g. sputtering processes and defect formation [69, 124]. At high energies, the interaction with the target electronic system has been already early modelled successfully by Bethe [125] with subsequent further improvements [126–128]. Towards lower energies, interaction becomes more complex even for the lightest ions, as details of the electronic structure of the material were predicted to affect the energy deposition [129]. These effects of the density of states of the irradiated material were later been confirmed in several experiments for metals with excitation thresholds for specific electronic states [130, 131] as well as for insulators featuring a band gap [132, 133]. Both phase effects [134], and even more relevant strong effects arising from chemical disorder [135] have been reported. They are important in complex material systems at the PFC surface

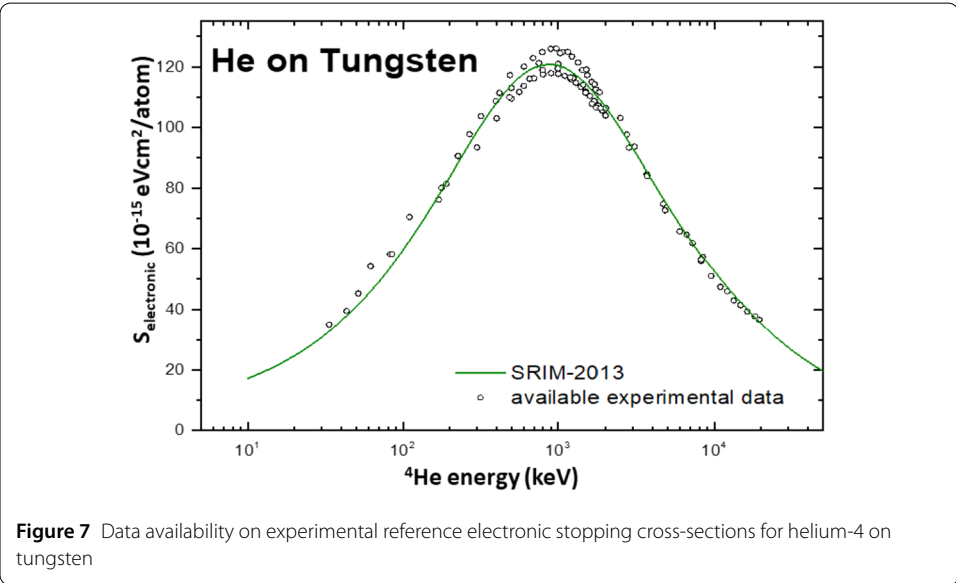
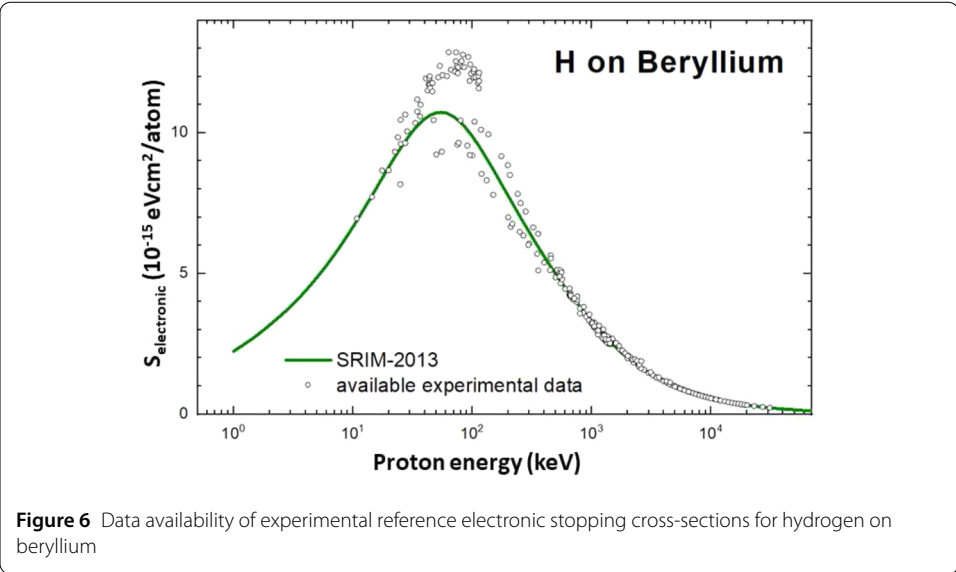
modified due to constant erosion and re-deposition. For light ions different from protons, also projectile excitation becomes increasingly relevant [136, 137] still challenging predictions up to date [138, 139]. In a similar fashion as calculations feature an increasing complexity towards low ion energies, the same applies to experiments: stopping powers are experimentally most straightforwardly obtained in transmission experiments [140], for which, at lower energies, however the deteriorating influence of surface contaminations increases. In backscattering geometry, effects of surface contamination are drastically reduced, however, at lower energies, effects of plural and multiple scattering affect the spectra, complicating the analysis, requiring accurate simulations [141, 142]. An additional option, available when sufficiently thin films of the target material cannot reliably be obtained is evaluation from the height of a spectrum recorded for a thicker film or bulk of the material of interest [143]. In all cases, however, material purity is of utmost importance, which is challenging to guarantee for thin layers near a surface [144]. For all the reasons above, the database of electronic stopping powers hosted by IAEA [145, 146] features only a limited number of datasets at low ion energies. Also, the materials, for which stopping powers have been measured or calculated is found limited [147]. The most commonly employed source for tabulated stopping powers, the semi empirical SRIM-code [148], is thus challenged in its predictive capacity. For many aspects of research on plasma-wall interaction is it, however, these low energies, which are most relevant. Low ion energies are not only relevant to model sputtering, fuel retention or defect formation, but are similarly necessary for quantification in analytical approaches such as Low- and Medium Energy Ion Scattering (LEIS & MEIS) [122, 149]. Table 3, summarizes the status quo for a number of elemental target materials highly relevant for next generation fusion devices, indicating the almost complete absence of data at low energies, as well as the presence of an ambiguity of available data.

Plots in Figs. 6 and 7, show respectively detailed data for H in Be and He in W, thus illustrating the limited availability and reliability of reference data at intermediate energies or their complete absence at low energies respectively. Recently, the development of new computational approaches such as time-dependent density functional theory [150, 151] or abandoning the modelling of a homogeneous electron gas [152] provides successively better predictions for specific systems, but commonly with high computational expenses. Dedicated experiments providing a better insight into the dependence of stopping powers on  $Z_2$  [153] or specifically targeting materials for PFMC [154] enhance simultaneously the predictive power of semi-empirical approaches. Nevertheless, due to the large number of relevant ion-target combinations, energies and experimental approaches, a concerted

**Table 3** Account on availability of the stopping powers data for selected elements

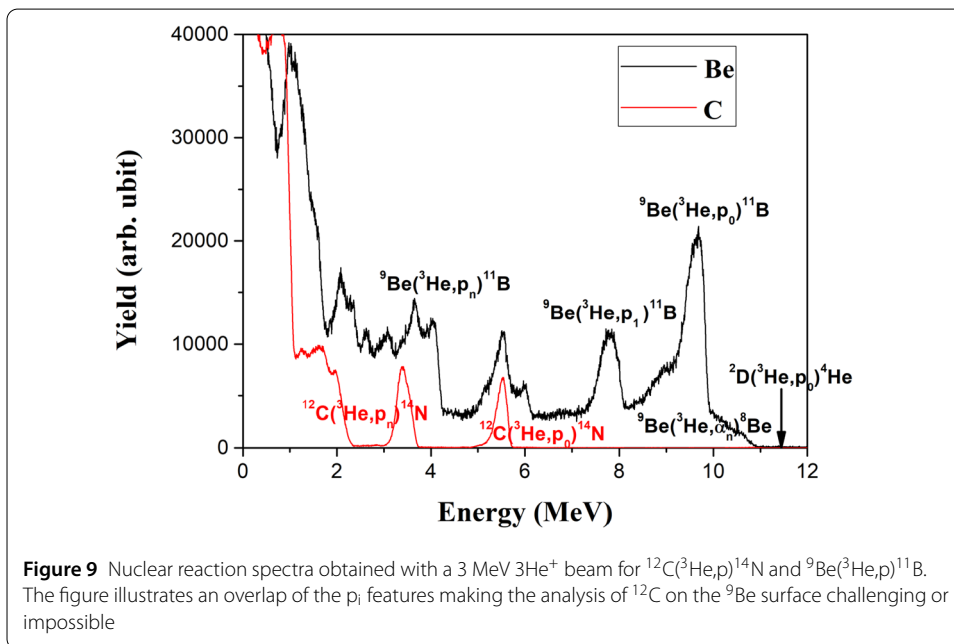
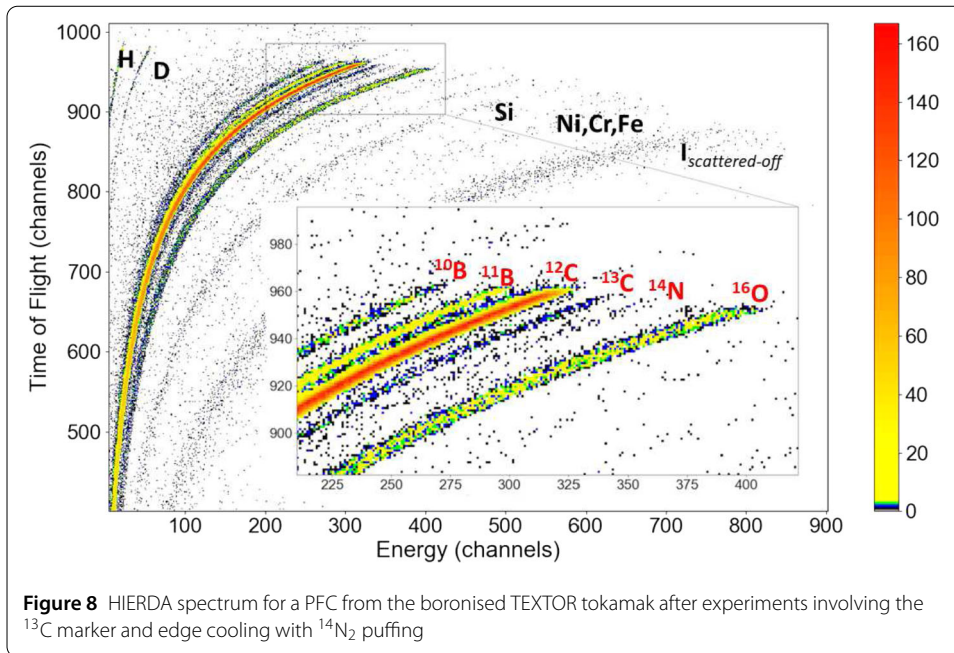
Element	H ions	He ions
Be	No data below 10 keV – no reliable data below 1 MeV.	No data below 200 keV.
C	High number of datasets	High number of datasets; limitations at low energies.
Mo	No data below 50 keV – data spread in the stopping maximum.	Only one low-energy dataset – spread in the stopping maximum.
W	Only one dataset below 100 keV.	Only one dataset below 300 keV; two datasets differing by 10% at classical IBA energies.





action - as proposed by a number of research groups in the CRP-F11023 coordinated by IAEA - will be necessary to build up comprehensive knowledge for the relevant materials in the relevant energy range on the stopping of H and He in Be, Fe, Mo and W.

Stopping powers are crucial for depth profiling, while scattering, recoil and reaction cross-sections are crucial for the quantification of the number and areal density of the target constituents. In other words, for quantitative material analysis stopping powers need to be combined with cross-sections. E. Rutherford [155] first suggested viewing the incoming particle and nucleus as small positively charged particles that interacts by Coulomb interaction and can very accurately be used to model the interactions in RBS that is named after him. This has since been complemented by a screening function, as suggested by [156, 157], which accounts for the fact that distance of interactions between the incoming ion and target atom will be so large that some electrons would effectively shield the nucleus. This is the situation for HIERDA where all elements can be detected. It is shown



in Fig. 8 for a PFC surface composition following experiments in the boronised TEXTOR tokamak (carbon wall machine) [158] involving the injection of  $^{13}\text{C}$  material migration marker and plasma edge cooling with  $^{14}\text{N}_2$ . However, the technique effectively traces only a very surface layer, while thicker layers are often to be examined.

At energies were the closest distance between the two particles becomes small, the strong interaction must also be taken into account. In such situation all different interactions must be considered separately thus complicating the analysis. An example is in Fig. 9 showing a “forest” of peaks in the spectra recorded in separate studies of Be and C. The

spectrum of protons emerging from the  $^{12}\text{C}(^3\text{He},\text{p})^{14}\text{N}$  process is “hidden” in the products of the  $^9\text{Be}(^3\text{He},\text{p})^{11}\text{B}$  reaction.

For light species nuclear reaction cross-sections are crucial, especially those for  $^3\text{He}$ -induced processes with  $^7\text{Li}$ ,  $^9\text{Be}$ ,  $^{10}\text{B}$ ,  $^{11}\text{B}$ ,  $^{12}\text{C}$ ,  $^{13}\text{C}$ , also  $^{14}\text{N}$ ,  $^{15}\text{N}$  and  $^{16}\text{O}$  in the 1-6 MeV energy range. That list takes into account isotopes used for PFC materials, wall conditioning agents, plasma edge cooling and most common impurity species. It is worth noting that the need for data for low- $Z$  atoms stems not only from the PFC studies, but also in medical research (radiotherapy) and space radiation protection [159]. The cross sections for these interactions cannot be calculated analytically but requires a large set of measurements. In some situation old cross sections originally measured to explore the structure of the nucleus [160] can be repurposed but there is still an ongoing development to increase the data sets [161–164]. For instance, the  $^9\text{Be}(^3\text{He},\text{p})^{11}\text{B}$  reaction had been studied already in the fifties of the 20th century at the projectile energy of 4.5 MeV [160] and, new data sets have been recently published: at  $135^\circ$  in the 1 - 2.5 MeV range [161] and from  $107^\circ$  -  $164^\circ$  in the 1.8 - 2.7 MeV range [162]. A data base for elastic (non-Rutherford) backscattering cross-sections is also important and, it is growing [165, 166]. For organising the available datasets IAEA has created the IBANDL database [167] and for some selected combination of particles of the existing cross sections has been combined with models of the interactions in the SigmaCalc [168] program that for limited some reactions can provide very good cross-sections.

## 5 Concluding remarks

The accelerator-based analysis and modification of materials is not an isolated or a passive strand of fusion research. The results directly contribute to decisions regarding the wall composition and diagnostic planning in the current and future devices, e.g. ITER and DEMO. It is a driving force for improvements and development of analytical capabilities (nuclear data sets, detectors, chambers) to ensure cutting edge research. To keep this status, continual development of the methods in accordance with what was outlined above is required. Especially the role of in-situ and in-operando systems for the material modification and analyses will be crucial for a deep insight into the dynamics of fuel retention and segregation of metals in materials relevant for PFC such as EUROFER.

### Acknowledgements

The authors are grateful to Mr. Jonas Åström, Mr. Bart Royeaerd and Mr. Sven Cederberg for the technical support in the accelerator operation during IBA measurements.

### Funding

The work has been supported by the Swedish Research Council (VR), Grant 2016–05380. Financial support of the Tandem Accelerator Infrastructure by VR-RFI (contract #2017–00646\_9) as well as the Swedish Foundation for Strategic Research (SSF) under contract RIF14–0053 is gratefully acknowledged. Open access funding provided by Royal Institute of Technology.

### Abbreviations

AMS, Accelerator Mass Spectroscopy; EPS, Enhanced Proton Scattering; EBS, Elastic Backscattering Spectroscopy; ERDA, Elastic Recoil Detection Analysis; GDOES, Glow Discharge Optical Emission Spectroscopy; GIC, Gas Ionization Chamber (detector); HIERDA, Heavy Ion ERDA; IBA, Ion Beam Analysis; ILW, ITER-Like Wall; JET, Joint European Torus; JET-C, JET with Carbon wall; JET-ILW, JET with ITER-Like Wall; LEIS, Low Energy Ion Source; LIAS, Laser-Induced Ablation Spectroscopy; LIBS, Laser-Induced Breakdown Spectroscopy; LID, Laser-Induced Desorption; NRA, Nuclear Reaction Analysis; PFC, Plasma-Facing Components; PFM, Plasma-Facing Materials; RBS, Rutherford Backscattering Spectrometry; RF, Radio Frequency; RGA, Residual Gas Analyser; RH, Remote Handling; SIGMA, Set-up for In-situ Growth, Material modification and Analysis; SIMS, Secondary Ion Mass Spectroscopy; TDS, Thermal Desorption Spectroscopy; ToF-ERDA, Time-of-Flight ERDA/HIERDA.



**Availability of data and materials**

No supplementary material is available.

**Declarations****Competing interests**

The authors declare no competing interests.

**Author contributions**

MR, DP and PP – conceptualisation, ion beam measurements, writing respective sections of the paper; SC and AW – discussions, structuring, reviewing the manuscript. All authors read and approved the final manuscript.

**Author details**

<sup>1</sup>Department of Plasma Physics, KTH Royal Institute of Technology, Stockholm, Sweden. <sup>2</sup>Department of Physics and Astronomy, Uppsala University, Uppsala, Sweden. <sup>3</sup>International Atomic Energy Agency, Vienna, Austria. <sup>4</sup>Culham Centre for Fusion Energy, Abingdon, Oxfordshire, United Kingdom.

**Publisher's Note**

Springer Nature remains neutral with regard to jurisdictional claims in published maps and institutional affiliations.

Received: 18 November 2022 Accepted: 9 February 2023 Published online: 24 February 2023

**References**

1. Wesson J. Tokamaks. 3rd ed. London: Oxford University Press; 2008.
2. Bosch H-S, Halle GM. Improved formulas for fusion cross-sections and thermal reactivities. Nucl Fusion. 1992;32:611–32. <http://iopscience.iop.org/article/10.1088/0029-5515/32/4/107/pdf>.
3. Moses E. Advances in inertial confinement fusion at the National Ignition Facility (NIF). Fusion Eng Des. 2010;85:983. <https://doi.org/10.1016/j.fusengdes.2009.11.006>.
4. Hoffman I. Review of accelerator driven heavy ion nuclear fusion. Matter Radiat Extrem. 2018;3:1. <https://doi.org/10.1016/j.mre.2017.12.001>.
5. Miyamoto K. Plasma physics for controlled fusion. Springer series on atomic, optical, and plasma physics. vol. 92. Berlin: Springer; 2016.
6. Artsimovitch LA. Tokamak devices. Nucl Fusion. 1972;12:215–51. <https://doi.org/10.1088/0029-5515/12/2/012>.
7. Spitzer L. The stellarator concept. Phys Fluids. 1958;1:253–64. <https://doi.org/10.1063/1.1705883> and <http://www-naweb.iaea.org/napc/physics/2ndgenconf/data/Reports/Spitzer%20Report.pdf>.
8. Federici G, Skinner CH, Brooks JN et al. Plasma-material interactions in current tokamaks and their implications for next step fusion reactors. Nucl Fusion. 2001;41:1967–2137. <https://doi.org/10.1088/0029-5515/41/12/218>.
9. Tanabe T, editor. Tritium: fuel of fusion reactors. Berlin: Springer; 2016.
10. Rubel M. Fusion neutrons: tritium breeding and impact on wall materials and components of diagnostic systems. J Fusion Energy. 2019;38:315–29.
11. Hofer WO, Roth J, editors. Physical processes of the interaction of fusion plasmas with solids. New York: Academic Press; 1996.
12. Naujoks D. Plasma-material interactions in controlled fusion. Berlin: Springer; 2006.
13. Philipps V, Wienhold P, Kirschner A, Rubel M. Erosion and redeposition of wall material in controlled fusion devices. Vacuum. 2002;67:399–408. [https://doi.org/10.1016/S0042-207X\(02\)00238-5](https://doi.org/10.1016/S0042-207X(02)00238-5).
14. Skinner CH, Amareescu E, Ascione G et al. Plasma wall interaction and tritium retention in TFTR. J Nucl Mater. 1977;241–243:214–26. [https://doi.org/10.1016/S0022-3115\(97\)80041-4](https://doi.org/10.1016/S0022-3115(97)80041-4).
15. Skinner CH, Gentile CA, Hosea JC et al. Tritium experience in large tokamaks: application to ITER. Nucl Fusion. 1999;39:271–92. <https://doi.org/10.1088/0029-5515/39/2/410>.
16. Keilhacker M, Watkins ML, JET Team. D-T experiments in the JET tokamak. J Nucl Mater. 1999;266–269:1–13. [https://doi.org/10.1016/S0022-3115\(98\)00811-3](https://doi.org/10.1016/S0022-3115(98)00811-3).
17. Andrew P, Brennan PD, Coad JP et al. Tritium retention and clean-up in JET. Fusion Eng Des. 1999;47:233–45. [https://doi.org/10.1016/S0920-3796\(99\)00084-8](https://doi.org/10.1016/S0920-3796(99)00084-8).
18. Coad JP, Bekris N, Elder JD et al. Erosion/deposition issues in JET, erosion/deposition issues at JET. J Nucl Mater. 2001;290–293:224–30. [https://doi.org/10.1016/S0022-3115\(00\)00479-7](https://doi.org/10.1016/S0022-3115(00)00479-7).
19. Penzhorn R-D, Bekris N, Berndt U et al. Tritium depth profiles in graphite and carbon fibre composite material exposed to tokamak plasmas. J Nucl Mater. 2001;288:170–8. [https://doi.org/10.1016/S0022-3115\(00\)00705-4](https://doi.org/10.1016/S0022-3115(00)00705-4).
20. Rubel M, Coad JP, Bekris N et al. Beryllium and carbon films in JET following D-T operation. J Nucl Mater. 2003;313–316:321–6. [https://doi.org/10.1016/S0022-3115\(02\)01350-8](https://doi.org/10.1016/S0022-3115(02)01350-8).
21. Coad JP, Rubel M, Likonen J et al. Material migration and fuel retention studies during the JET carbon divertor campaigns. Fusion Eng Des. 2018;138:78–108. <https://doi.org/10.1016/j.fusengdes.2018.10.002>.
22. Counsell GC, Coad JP, Grisola C et al. Tritium retention in next step devices and the requirements for mitigation and removal techniques. Plasma Phys Control Fusion. 2006;48:B189–99. <https://doi.org/10.1088/0741-3335/48/12B/S18>.
23. Ivanova D, Rubel M, Philipps V et al. Laser-based and thermal methods for fuel removal and cleaning of plasma-facing components. J Nucl Mater. 2011;415:S801–S-804. <https://doi.org/10.1016/j.jnucmat.2011.01.119>.
24. Rubel M, De Temmerman G, Sergienko G et al. Fuel removal from plasma-facing components by oxidation-assisted technique. An overview of surface morphology after oxidation. J Nucl Mater. 2007;363–365:877–81. <https://doi.org/10.1016/j.jnucmat.2007.01.107>.
25. Hopf C, Rohde V, Jacob W et al. Oxygen glow discharge cleaning in ASDEX upgrade. J Nucl Mater. 2007;363–365:882–7. <https://doi.org/10.1016/j.jnucmat.2007.01.108>.

26. Roth J, Tsitroni E, Loarer T et al. Tritium inventory in ITER plasma-facing materials and tritium removal procedures. *Plasma Phys Control Fusion*. 2008;50:103001. <https://doi.org/10.1088/0741-3335/50/10/103001>.
27. Rubel M, Ivanova D, Philipps V et al. Efficiency of fuel removal techniques tested on plasma-facing components from the TEXTOR tokamak. *Fusion Eng Des*. 2012;87:935–40. <https://doi.org/10.1016/j.fusengdes.2012.02.054>.
28. Matthews GF, Edwards P, Hirai T et al. ITER-like wall project overview. *Phys Scr T*. 2007;128:137–43. <https://doi.org/10.1088/0031-8949/2007/T128/027>.
29. Matthews GF, Edwards P, Greuner H et al. Current status of the JET ITER-like wall project. *Phys Scr T*. 2010;138:014030. <https://doi.org/10.1088/0031-8949/2009/T138/014030>.
30. Matthews GF, Beursknes M, Brezinsek S et al. Overview of the ITER-like wall project. *Phys Scr T*. 2011;145:014001. <https://doi.org/10.1088/0031-8949/2011/T145/014001>.
31. Rubel M, Bailescu V, Coad JP et al. Beryllium plasma-facing components for the ITER-like wall project at JET. *Inst Phys Conf Ser*. 2008;100:062028. <https://doi.org/10.1088/1742-6596/100/6/062028>.
32. Maier H, Hirai T, Rubel M et al. Tungsten and beryllium armour development for the JET ITER-like wall project. *Nucl Fusion*. 2007;47:222–7. <https://doi.org/10.1088/0029-5515/47/3/009>.
33. Mertens P, Philipps V, Pintsuk G et al. Clamping of solid tungsten components for the bulk W divertor row in JET—precautionary design for a brittle material. *Phys Scr T*. 2009;138:014032. <https://doi.org/10.1088/0031-8949/2009/T138/014032>.
34. Mertens P. Detailed design of a solid tungsten divertor row for JET in relation to the physics goals. *Phys Scr T*. 2011;145:014002. <https://doi.org/10.1088/0031-8949/2011/T145/014002>.
35. Matthews GF. Plasma operation with an all metal first-wall: comparison of an ITER-like wall with a carbon wall in JET. *J Nucl Mater*. 2013;438:S2–10. <https://doi.org/10.1016/j.jnucmat.2013.01.282>.
36. Loarer T, Brezinsek S, Philipps V et al. Comparison of fuel retention in JET between carbon and the ITER-like wall. *J Nucl Mater*. 2013;438:S108–13. <https://doi.org/10.1016/j.jnucmat.2013.01.017>.
37. Widdowson A, Coad JP, Alves E et al. Overview of fuel inventory in JET with the ITER-like wall. *Nucl Fusion*. 2017;57:086045. <https://doi.org/10.1088/1741-4326/aa7475>.
38. Widdowson A, Alves E, Baron-Wiecheč A et al. Overview of the JET ITER-like wall divertor. *Nucl Mater Energy*. 2017;12:499–505. <https://doi.org/10.1016/j.nme.2016.12.008>.
39. Widdowson A, Alves E, Baron-Wiecheč A et al. Fuel inventory and material migration of JET main chamber plasma facing components compared over three operational periods. *Phys Scr T*. 2020;171:014051. <https://doi.org/10.1088/1402-4896/ab5350>.
40. Mayer M, Krat S, Van Renteghem W et al. Erosion and deposition in the JET divertor during the first ILW campaign. *Phys Scr T*. 2016;167:014051. <https://doi.org/10.1088/0031-8949/T167/1/014051>.
41. Krat S, Mayer M, Baron-Wiecheč A et al. Comparison of erosion and deposition in JET divertor during the first three ITER-like wall campaigns. *Phys Scr T*. 2020;171:014059. <https://doi.org/10.1088/1402-4896/ab5c11>.
42. Baron-Wiecheč A, Widdowson A, Alves E et al. Global erosion and deposition patterns in JET with the ITER-like wall. *J Nucl Mater*. 2015;463:157–61. <https://doi.org/10.1016/j.jnucmat.2015.01.038>.
43. Widdowson A, Alves E, Ayres CF et al. Material migration patterns and overview of first surface analysis of the JET ITER-like wall. *Phys Scr T*. 2014;159:014010. <https://doi.org/10.1088/0031-8949/2014/T159/014010>.
44. Baron-Wiecheč A, Fortuna-Zalešna E, Grzonka J et al. First dust study in JET with the ITER-like wall: sampling, analysis and classification. *Nucl Fusion*. 2015;55:113033. <http://stacks.iop.org/0029-5515/55/113033>.
45. Fortuna-Zalešna E, Weckmann A, Grzonka J et al. Dust survey following the final shutdown of TEXTOR: metal particles and fuel retention. *Phys Scr T*. 2016;167:014059. <https://doi.org/10.1088/0031-8949/T167/1/014059>.
46. Fortuna-Zalešna E, Grzonka J, Rubel M et al. Studies of dust from JET with the ITER-like wall: composition and internal structure. *Nucl Mater Energy*. 2017;12:582–7. <https://doi.org/10.1016/j.nme.2016.11.027>.
47. Litaudon X, Contributors JET. Overview of the JET in support of ITER. *Nucl Fusion*. 2017;57:102001. <https://doi.org/10.1088/1741-4326/aa5e28>.
48. Rubel M, Widdowson A, Grzonka J et al. Dust generation in tokamaks: overview of beryllium and tungsten dust characterisation in JET with the ITER-like wall. *Fusion Eng Des*. 2018;136:579–86. <https://doi.org/10.1016/j.fusengdes.2018.03.027>.
49. Merola M, Escubriac F, Raffray R et al. Overview and status of ITER internal components. *Fusion Eng Des*. 2014;89:890–5. <https://doi.org/10.1016/j.fusengdes.2014.01.055>.
50. Tsitroni E, Pégourié B, Marandet Y et al. Multi machine scaling of fuel retention in 4 carbon dominated tokamaks. *J Nucl Mater*. 2011;415:S735–9. <https://doi.org/10.1016/j.jnucmat.2011.01.132>.
51. Wampler WR, Bastasz R, Buchenauer D et al. Erosion and deposition of metals and carbon in the DIII-D divertor. *J Nucl Mater*. 1999;266–269:791–7. [https://doi.org/10.1016/S0022-3115\(96\)00196-1](https://doi.org/10.1016/S0022-3115(96)00196-1).
52. Allen SL, Wampler WR, Mclean AG et al. <sup>13</sup>C transport studies in L-mode divertor plasmas on DIII-D. *J Nucl Mater*. 2005;337–339:30–4. <https://doi.org/10.1016/j.jnucmat.2004.09.066>.
53. Loarer T, Brosset C, Bucalossi J et al. Gas balance and fuel retention in fusion devices. *Nucl Fusion*. 2007;47:1112–20. <https://doi.org/10.1088/0029-5515/47/9/007>.
54. Masaki K, Sugiyama K, Tanabe T et al. Tritium distribution in the JT-60 W-shaped divertor. *J Nucl Mater*. 2003;313–316:514–8. [https://doi.org/10.1016/S0022-3115\(02\)01388-0](https://doi.org/10.1016/S0022-3115(02)01388-0).
55. Jitkamada Y, Di Pietro E, Hanada M et al. Completion of JT-60SA construction and contribution to ITER. *Nucl Fusion*. 2022;62:042002. <https://doi.org/10.1088/1741-4326/ac10e7>.
56. Tokitani M, Masuzaki S, Yoshida N et al. Microstructural characterization of mixed-material deposition layer on the LHD divertor tiles by using nano-geological diagnosis. *J Nucl Mater*. 2013;438:S818–21. <https://doi.org/10.1016/j.jnucmat.2013.01.177>.
57. Mayer M, Balden M, Brezinsek S et al. Material erosion and deposition on the divertor of W7-X. *Phys Scr T*. 2020;171:014035. <https://doi.org/10.1088/1402-4896/ab4b8c>.
58. Brezinsek S, Dhard CP, Jakubowski M et al. Plasma-surface interaction in the stellarator W7-X: conclusion drawn from operation with graphite plasma-facing components. *Nucl Fusion*. 2022;62:016006. <https://doi.org/10.1088/1741-4326/ac3508>.
59. Brezinsek S, Widdowson A, Mayer M et al. Beryllium migration in JET ITER-like wall plasmas. *Nucl Fusion*. 2015;55:063021. <https://doi.org/10.1088/0029-5515/55/6/063021>.

60. Neu R, Kallenbach A, Balden M et al. Overview on plasma operation with a full tungsten wall in ASDEX upgrade. *J Nucl Mater.* 2013;438:534–41. <https://doi.org/10.1016/j.jnucmat.2013.01.006>.
61. Neu R, Dux R, Geier A et al. Impurity behaviour in the ASDEX upgrade divertor tokamak with large area tungsten walls. *Plasma Phys Control Fusion.* 2002;41:811–26. <https://doi.org/10.1088/0741-3335/44/6/313>.
62. Brezinsek S, Kirschner A, Mayer M et al. Erosion, screening and migration of tungsten in the JET divertor. *Nucl Fusion.* 2019;59:096035. <https://doi.org/10.1088/1741-4326/ab2aef>.
63. Rubel M, De Temmerman G, Coad JP et al. Mirror test for ITER at the JET tokamak: an overview of the programme. *Rev Sci Instrum.* 2006;77:063501. <https://doi.org/10.1063/1.2202915>.
64. Ivanova D, Rubel M, Widdowson A et al. An overview of the comprehensive first mirrors test in JET with ITER-like wall. *Phys Scr T.* 2014;159:014011. <https://doi.org/10.1088/0031-8949/2014/T159/014011>.
65. Moon S, Petersson P, Rubel M et al. First mirror test in JET for ITER: complete overview after three ILW campaigns. *Nucl Mater Energy.* 2019;19:59–66. <https://doi.org/10.1016/j.nme.2019.02.009>.
66. Litnovsky A, Voitsenya VS, Reichle R et al. Diagnostic mirrors for ITER: research in a frame of international tokamak physics activity. *Nucl Fusion.* 2019;59:066029. <https://doi.org/10.1088/1741-4326/ab1446>.
67. Rubel M, Moon S, Petersson P et al. First mirror erosion-deposition studies in JET using an ITER-like mirror test assembly. *Nucl Fusion.* 2021;61:046022. <https://doi.org/10.1088/1741-4326/abdb92>.
68. Chu WK, Mayer M, Nicolet MA. Backscattering spectroscopy. New York: Academic Press; 1978.
69. Tesmer JR, Nastasi M, editors. Handbook of modern ion beam analysis. Pittsburg: Material Research Society; 1995.
70. Rubel M. Analysis of plasma facing materials: material migration and fuel retention. *Phys Scr T.* 2006;123:54–65. <https://doi.org/10.1088/0031-8949/2006/T123/007>.
71. Rubel M, Coad JP, Likonen J, Philipps V. The role and application of ion beam analysis for studies of plasma-facing components in controlled fusion devices. *Nucl Instrum Methods Phys Res, Sect B, Beam Interact Mater Atoms.* 2016;371:4–11. <https://doi.org/10.1016/j.nimb.2015.09.077>.
72. Mayer M, Möller S, Rubel M et al. Ion beam analysis of fusion plasma-facing materials and components: facilities and research challenges. *Nucl Fusion.* 2020;60:025001. <https://doi.org/10.1088/1741-4326/ab5817>.
73. Mayer M, Gauthier E, Sugiyama K, von Toussaint U. Quantitative depth profiling of deuterium up to very large depths. *Nucl Instrum Methods Phys Res, Sect B, Beam Interact Mater Atoms.* 2009;267:506–12. <https://doi.org/10.1016/j.nimb.2008.11.033>.
74. Rubel M, Petersson P, Zhou Y et al. Fuel inventory and deposition in castellated structures in JET-ILW. *Nucl Fusion.* 2017;57:066027. <https://doi.org/10.1088/1741-4326/aa6864>.
75. Dittrich L, Petersson P, Rubel M et al. Fuel retention and erosion-deposition on inner wall cladding tiles in JET-ILW. *Phys Scr.* 2021;96:124071. <https://doi.org/10.1088/1402-4896/ac379e>.
76. Widdowson A, Coad JP, Zayachuk Y et al. Evaluation of tritium retention in plasma facing components during JET tritium operations. *Phys Scr.* 2021;96:124075. <https://doi.org/10.1088/1402-4896/ac3b30>.
77. Ström P, Petersson P, Rubel M et al. Analysis of co-deposited layers with deuterium and impurity elements on samples from the divertor of JET with ITER-like wall. *J Nucl Mater.* 2019;516:202–13. <https://doi.org/10.1016/j.jnucmat.2018.11.027>.
78. Garcia-Carrasco A, Möller S, Petersson P et al. Impact of ion cyclotron wall conditioning on plasma-facing components. *Phys Scr T.* 2014;159:014017. <https://doi.org/10.1088/0031-8949/2014/T159/014017>.
79. Pégourié B, Panayotis S, Languille P et al. Deuterium inventory in Tore Supra: coupled carbon – deuterium balance. *J Nucl Mater.* 2013;438:S120–6. <https://doi.org/10.1016/j.jnucmat.2013.01.019>.
80. Rubel M, Brezinsek S, Widdowson A. Surface modification by fusion plasmas. Plasma applications for material modification: from microelectronics to biological materials. Singapore: Jenny Stanford Publishing; 2020.
81. Bykov I, Petersson P, Bergsäter H et al. Investigation of tritium analysis methods for ion microbeam application. *Nucl Instrum Methods Phys Res, Sect B, Beam Interact Mater Atoms.* 2012;273:250–3. <https://doi.org/10.1016/j.nimb.2011.07.087>.
82. Kubota N et al. Surface analysis for FTFR armour tile exposed to D-T plasmas using nuclear technique. In: 21st IAEA conf. on fusion energy, EX/P4-12; 2006. [https://www-pub.iaea.org/MTCD/Meetings/FEC2006/ex\\_p4-12.pdf](https://www-pub.iaea.org/MTCD/Meetings/FEC2006/ex_p4-12.pdf).
83. Friedrich M, Pilz W, Sun G et al. Tritium depth profiling by AMS in carbon samples from fusion experiments. *Phys Scr T.* 2001;94:98–101. <https://doi.org/10.1238/Physica.Topical.094a00098>.
84. Dittrich L, Petersson P, Moon S. Retention of seeded gases in first wall components from the JET tokamak with the ITER-like wall. In: 32nd symposium on fusion technology. Dubrovnik, Croatia. 2022.
85. Lagoyannis A, Tsavalas P, Mergia K et al. Surface analysis of the ITER-like wall divertor tiles at JET tokamak. *Nucl Fusion.* 2017;57:076027. <https://doi.org/10.1088/1741-4326/aa6ec1>.
86. Bykov I, Bergsäter H, Possnert G et al. Studies of Be migration in the JET tokamak using AMS with <sup>10</sup>Be marker. *Nucl Instrum Methods Phys Res, Sect B, Beam Interact Mater Atoms.* 2016;371:370–5. <https://doi.org/10.1016/j.nimb.2015.12.007>.
87. Gudowska I, Bergsäter H, Emmoth B et al. Fluxes of boron in the scrape-off plasma of TEXTOR following boronization. *J Nucl Mater.* 1990;176–177:363–9. [https://doi.org/10.1016/0022-3115\(90\)90073-V](https://doi.org/10.1016/0022-3115(90)90073-V).
88. Hakola A, Likonen J, Koivuranta S et al. Global transport of light elements boron and carbon in the full-W ASDEX upgrade. *J Nucl Mater.* 2011;415:S227–30. <https://doi.org/10.1016/j.jnucmat.2010.08.053>.
89. Ström P, Petersson P, Rubel M et al. Characterisation of layers formed on plasma-facing components in controlled fusion devices: role of heavy ion elastic recoil detection. *Vacuum.* 2015;122:260–7. <https://doi.org/10.1016/j.vacuum.2015.04.019>.
90. Weckmann A, Petersson P, Rubel M et al. Review of global migration, fuel retention and modelling after TEXTOR decommission. *Nucl Mater Energy.* 2018;17:83–112. <https://doi.org/10.1016/j.nme.2018.09.003>.
91. Weckmann A, Petersson P, Varju J et al. Deuterium deposition patterns for fuel retention in the divertor of the COMPASS tokamak. *Fusion Eng Des.* 2022;179:113118. <https://doi.org/10.1016/j.fusengdes.2022.113118>.
92. Coad JP, Rubel M, Wu CH. The amount and distribution of deuterium retained in the JET divertor after the C and Be phases in 1994-5. *J Nucl Mater.* 1997;241–243:408–13. [https://doi.org/10.1016/S0022-3115\(97\)80073-6](https://doi.org/10.1016/S0022-3115(97)80073-6).
93. Rubel M, Coad JP, Hole D. Accelerator-based ion beam analysis of fusion reactor materials. *Vacuum.* 2005;78:255–61. <https://doi.org/10.1016/j.vacuum.2005.01.109>.

94. Rubel M, Coad JP, Stenström K et al. Overview of tracer techniques in studies of material erosion, re-deposition and fuel inventory in tokamaks. *J Nucl Mater.* 2004;329–333:795–9. <https://doi.org/10.1016/j.jnucmat.2004.04.154>.
95. Coad JP, Likonen J, Rubel M et al. Overview of material re-deposition and fuel retention studies at JET with the gas box divertor. *Nucl Fusion.* 2006;46:350–66. <https://doi.org/10.1088/0029-5515/46/2/018>.
96. Petersson P, Rubel M, Possnert G et al. Nuclear reaction and heavy ion ERD analysis of wall materials from controlled fusion devices: deuterium and nitrogen 15 studies. *Nucl Instrum Methods Phys Res, Sect B, Beam Interact Mater Atoms.* 2012;273:212. <https://doi.org/10.1016/j.nimb.2011.07.053>.
97. Rubel M, Philipps V, Marot L et al. Nitrogen and neon retention in plasma-facing materials. *J Nucl Mater.* 2011;415:S223–6. <https://doi.org/10.1016/j.jnucmat.2010.08.035>.
98. Petersson P, Rubel M, Possnert G et al. Injection of nitrogen-15 tracer into ASDEX upgrade: new technique in material migration studies. *J Nucl Mater.* 2013;438:S616–9. <https://doi.org/10.1016/j.jnucmat.2013.01.129>.
99. Rubel M, Wienhold P, Almqvist N et al. Silicon fluxes in the scrape-off layer plasma during silicon-assisted operation of TEXTOR. *J Nucl Mater.* 1995;220–222:536–40. [https://doi.org/10.1016/0022-3115\(94\)00535-4](https://doi.org/10.1016/0022-3115(94)00535-4).
100. Ström P, Petersson P, Arredondo Parra R et al. Sputtering of polished EUROFER97 steel: surface structure modification with tungsten and tantalum. *J Nucl Mater.* 2018;508:139. <https://doi.org/10.1016/j.jnucmat.2018.05.031>.
101. Ström P, Primetzhofner D, Schwarz-Selinger T, Sugiyama K. Compositional and morphological analysis of FeW films modified by sputtering and heating. *Nucl Mater Energy.* 2017;12:472–7. <https://doi.org/10.1016/j.nme.2017.03.002>.
102. Petersson P, Rubel M, Possnert G, Pégourié B. Micro distribution of fuel and metal in carbon based plasma-facing components. *Phys Scr T.* 2011;145:014014. <https://doi.org/10.1088/0031-8949/2011/T145/014014>.
103. Fazinić S, Provatás G, Božičević-Mihalić I et al. Dust monitors in JET with ITER-like wall for diagnosis of mobilized particles and co-deposited layers. *Materials.* 2022;15:8353. <https://doi.org/10.3390/ma15238353>.
104. Fazinić S, Tadić T, Vuksić M et al. Ion micro-beam analysis of dust particles and co-deposits from JET with ITER-like wall. *Anal Chem.* 2018;90:5744. <https://pubs.acs.org/doi/pdf/10.1021/acs.analchem.8b00073>.
105. Fazinić S, Božičević-Mihalić I, Provatás G et al. Micro-analyses of dust particles generated in the JET tokamak with the ITER-like wall. *Nucl Fusion.* 2020;60:12606. <https://doi.org/10.1088/1741-4326/abb53d>.
106. Mayer M, Philipps V, Wienhold P et al. Hydrogen inventories in nuclear fusion devices. *J Nucl Mater.* 2001;290–293:381–8. [https://doi.org/10.1016/S0022-3115\(00\)00486-4](https://doi.org/10.1016/S0022-3115(00)00486-4).
107. Loarer T, Brosset C, Bucalossi J et al. Gas balance and fuel retention in fusion devices. *Nucl Fusion.* 2007;47:1112–20. <https://doi.org/10.1088/0029-5515/47/9/007>.
108. Heinola K, Widdowson A, Likonen J et al. Long-term fuel retention in JET ITER-like wall. *Phys Scr T.* 2016;167:014075. <https://doi.org/10.1088/0031-8949/T167/1/014075>.
109. Summers DDD, Beurskens MNA, Coad JP et al. In-situ measurement of hydrogen retention in JET carbon tiles. *J Nucl Mater.* 2001;290–293:496–500. [https://doi.org/10.1016/S0022-3115\(00\)00481-5](https://doi.org/10.1016/S0022-3115(00)00481-5).
110. Huber A, Mayer M, Philipps V et al. In-situ measurement of trapped hydrogen by laser desorption in TEXTOR-94. *Phys Scr T.* 2001;94:102–5. <https://doi.org/10.1238/Physica.Topical.094a00102>.
111. Schweer B, Irek F, Sergienko G et al. In-situ diagnostic for monitoring of deuterium and tritium in re-deposited carbon layers by laser induced desorption. *J Nucl Mater.* 2007;363–365:1375–9. <https://doi.org/10.1016/j.jnucmat.2007.01.247>.
112. Philipps V, Malaquias A, Hakola A et al. Development of laser-based techniques for in-situ characterization of the first wall in ITER and future fusion devices. *Nucl Fusion.* 2013;53:093002. <https://doi.org/10.1088/0029-5515/53/9/093002>.
113. Malaquias M, Philipps V, Huber A et al. Development of ITER relevant laser techniques for deposited layer characterization and tritium inventory. *J Nucl Mater.* 2013;438:S936–9. <https://doi.org/10.1016/j.jnucmat.2013.01.203>.
114. Zlobinski M, De Temmerman G, Porosnicu C et al. Efficiency of layer-induced desorption of D from Be/D layers and surface modification due to LID. *Phys Scr T.* 2020;171:014075. <https://doi.org/10.1088/1402-4896/ab5ea1>.
115. Ström P, Petersson P, Rubel M, Possnert G et al. A combined segmented anode gas ionization chamber and time-of-flight detector for heavy ion elastic recoil detection analysis. *Rev Sci Instrum.* 2016;87:103303. <https://doi.org/10.1063/1.4963709>.
116. Garcia-Carrasco A, Petersson P, Hallén A et al. Impact of helium implantation and ion-induced damage on reflectivity of molybdenum mirrors. *Nucl Instrum Methods Phys Res, Sect B, Beam Interact Mater Atoms.* 2016;382:91–5. <https://doi.org/10.1016/j.nimb.2016.02.065>.
117. Rubel M, Moon S, Petersson P et al. Metallic mirrors for plasma diagnosis in current and future reactors: tests for ITER and DEMO. *Phys Scr T.* 2017;170:014061. <https://doi.org/10.1088/1402-4896/aa8e27>.
118. Schwarz-Selinger T. Deuterium retention in MeV self-implanted tungsten: influence of damaging dose rate. *Nucl Mater Energy.* 2017;12:683–8. <https://doi.org/10.1016/j.nme.2017.02.003>.
119. Widdowson A, Baron-Wiecheć A, Coad JP et al. Experience of handling beryllium, tritium and activated components from JET ITER like wall. *Phys Scr T.* 2016;167:014057. <https://doi.org/10.1088/0031-8949/T167/1/014057>.
120. Kantre K, Szabo PS, Moro MV et al. Combination of in-situ ion beam analysis and thermal desorption spectroscopy for studying deuterium implanted in tungsten. *Phys Scr.* 2021;96:124004. <https://doi.org/10.1088/1402-4896/ac1a88>.
121. Ström P, Primetzhofner D. Ion beam tools for nondestructive in-situ and in-operando composition analysis and modification of materials at the Tandem Laboratory in Uppsala. *J Instrum.* 2022;17:P04011. <https://doi.org/10.1088/1748-0221/17/04/P04011>.
122. Shams-Latifí J, Ström P, Pitthan E, Primetzhofner D. An in-situ ToF-LEIS and AES study of near-surface modifications of the composition of EUROFER97 induced by thermal annealing. *Nucl Mater Energy.* 2022;30:101139. <https://doi.org/10.1016/j.nme.2022.101139>.
123. Sigmund P. Particle penetration and radiation effects. vol. 2. Switzerland: Springer; 2014.
124. Sand AE, Nordlund K. *J Nucl Mater.* 2015;456:99–105.
125. Bethe H. Zur Theorie des Durchgangs schneller Korpuskularstrahlen durch Materie. *Ann Phys.* 1930;5:325–400. <https://doi.org/10.1002/andp.19303970303>.

126. Bethe H. Bremsformel für Elektronen relativistischer Geschwindigkeit. *Z Phys.* 1932;76:293–9. <https://doi.org/10.1007/BF01342532>.
127. Möller C. Zur Theorie des Durchgangs schneller Elektronen durch Materie. *Ann Phys.* 1932;406:531–85. <https://doi.org/10.1002/andp.19324060506>.
128. Bloch F. Zur Bremsung rasch bewegter Teilchen beim Durchgang durch Materie. *Ann Phys.* 1933;408:285–320. <https://doi.org/10.1002/andp.19334080303>. Bremsvermögen von Atomen mit mehreren Elektronen, *Z. Physik.* 1933;81:363–376. <https://doi.org/10.1103/PhysRevA.49.1083>.
129. Fermi E, Teller E. The capture of negative mesotrons in matter. *Phys Rev.* 1947;72:399–408. <https://doi.org/10.1103/PhysRev.72.399>.
130. Valdes JE, Arista NR. Energy loss of slow protons in solids: deviation from the proportionality with projectile velocity. *Phys Rev A.* 1994;49:1083–8–2695. <https://doi.org/10.1103/PhysRevA.49.2690>.
131. Markin SN, Primetzhofer D, Spitz M, Bauer P. Electronic stopping of low-energy H and He in Cu and Au investigated by time-of-flight low-energy ion scattering. *Phys Rev B.* 2009;80:205105. <https://doi.org/10.1103/PhysRevB.80.205105>.
132. Auth C, Mertens A, Winter H, Borisov A. Threshold in the stopping of slow protons scattered from the surface of a wide-band-gap insulator. *Phys Rev Lett.* 1999;81:4831–4. <https://doi.org/10.1103/PhysRevLett.81.4831>.
133. Markin SN, Primetzhofer D, Bauer P. Vanishing electronic energy loss of very slow light ions in insulators with large band gaps. *Phys Rev Lett.* 2009;103:113201. <https://doi.org/10.1103/PhysRevLett.103.113201>.
134. Bauer P, Kastner F, Arnau A et al. Phase effect in the energy loss of H projectiles in Zn targets: experimental evidence and theoretical explanation. *Phys Rev Lett.* 1992;69:1137–9. <https://doi.org/10.1103/PhysRevLett.69.1137>.
135. Quashie EE, Ullah R, Andrade X, Correa AA. Effect of chemical disorder on the electronic stopping of solid solution alloys. *Acta Mater.* 2020;196:576–83. <https://doi.org/10.1016/j.actamat.2020.06.061>.
136. Primetzhofer D, Mertens A, Winter H, Borisov A. Electronic excitations of slow ions in a free electron gas metal: evidence for charge exchange effects. *Phys Rev Lett.* 2011;107:163201. <https://doi.org/10.1103/PhysRevLett.107.163201>.
137. Lohmann S, Primetzhofer D. Disparate energy scaling of trajectory-dependent electronic excitations for slow protons and He ions. *Phys Rev Lett.* 2020;124:096601. <https://doi.org/10.1103/PhysRevLett.124.096601>.
138. Li C-K, Wang F, Liao B et al. Ab initio electronic stopping power and threshold effect of channeled slow light ions in HfO<sub>2</sub>. *Phys Rev B.* 2017;96:094301. <https://doi.org/10.1103/PhysRevB.96.094301>.
139. Quashie EE, Correa AA. Electronic stopping power of protons and alpha particles in nickel. *Phys Rev B.* 2018;98:235122. <https://doi.org/10.1103/PhysRevB.98.235122>.
140. Mertens P. How to measure absolute stopping cross sections by backscattering and transmission methods: part II. Transmission. *Nucl Instrum Methods Phys Res, Sect B, Beam Interact Mater Atoms.* 1987;27:315–22. [https://doi.org/10.1016/0168-583X\(87\)90570-2](https://doi.org/10.1016/0168-583X(87)90570-2).
141. Bauer P, Semrad D, Mertens P. Reference proton stopping cross sections for five elements around the maximum. *Nucl Instrum Methods Phys Res, Sect B, Beam Interact Mater Atoms.* 1985;12:56–61. [https://doi.org/10.1016/0168-583X\(86\)90259-4](https://doi.org/10.1016/0168-583X(86)90259-4).
142. Biersack JP, Steinbauer E, Bauer P. A particularly fast TRIM version for ion backscattering and high energy ion implantation. *Nucl Instrum Methods Phys Res, Sect B, Beam Interact Mater Atoms.* 1991;61:77–82. [https://doi.org/10.1016/0168-583X\(91\)95564-T](https://doi.org/10.1016/0168-583X(91)95564-T).
143. Roth D, Goebel D, Primetzhofer D, Bauer P. A procedure to determine electronic energy loss from relative measurements with TOF-LEIS. *Nucl Instrum Methods Phys Res, Sect B, Beam Interact Mater Atoms.* 2013;317:61–5. <https://doi.org/10.1016/j.nimb.2012.12.094>.
144. Roth D, Celedon CE, Goebel D et al. Systematic analysis of different experimental approaches to measure electronic stopping of very slow hydrogen ions. *Nucl Instrum Methods Phys Res, Sect B, Beam Interact Mater Atoms.* 2018;437:1–7. <https://doi.org/10.1016/j.nimb.2018.09.028>.
145. Stopping Power Database. Available at: <https://www-nds.iaea.org/stopping/>
146. Montanari CC, Dimitriou P. The IAEA stopping power database, following the trends in stopping power of ions in matter. *Nucl Instrum Methods Phys Res, Sect B, Beam Interact Mater Atoms.* 2017;408:50–5. <https://doi.org/10.1016/j.nimb.2017.03.138>.
147. Wittmaack K. Misconceptions impairing the validity of the stopping power tables in the SRIM library and suggestions for doing better in the future. *Nucl Instrum Methods Phys Res, Sect B, Beam Interact Mater Atoms.* 2016;380:57–70. <https://doi.org/10.1016/j.nimb.2016.04.057>.
148. Ziegler JF, Ziegler MD, Biersack JP. SRIM – the stopping and range of ions in matter (2010). *Nucl Instrum Methods Phys Res, Sect B, Beam Interact Mater Atoms.* 2010;268:1818–23. <https://doi.org/10.1016/j.nimb.2010.02.091>.
149. Koslowski HR, Bhattacharyya SR, Hansen P et al. Temperature-dependent in-situ LEIS measurement of W surface enrichment by 250 eV D sputtering of EUROFER. *Nucl Mater Energy.* 2018;16:181–90. <https://doi.org/10.1016/j.nme.2018.07.001>.
150. Schleife A, Kanai Y, Correa AA. Accurate atomistic first-principles calculations of electronic stopping. *Phys Rev B.* 2015;91:014306. <https://doi.org/10.1103/PhysRevB.91.014306>.
151. Ojanperä A, Krashennnikov AV, Puska M. Electronic stopping power from first-principles calculations with account for core electron excitations and projectile ionization. *Phys Rev B.* 2014;89:035120. <https://doi.org/10.1103/PhysRevB.89.035120>.
152. Matias F, Grande PL, Vos H et al. Nonlinear stopping effects of slow ions in a no-free-electron system: titanium nitride. *Phys Rev A.* 2019;100:030701. <https://doi.org/10.1103/PhysRevA.100.030701>.
153. Moro MV, Bauer P, Primetzhofer D. Experimental electronic stopping cross section of transition metals for light ions: systematics around the stopping maximum. *Phys Rev A.* 2022;102:022808. <https://doi.org/10.1103/PhysRevA.102.022808>.
154. Moro MV, Wolf PM, Bruckner B et al. Experimental electronic stopping cross section of tungsten for light ions in a large energy interval. *Nucl Instrum Methods Phys Res, Sect B, Beam Interact Mater Atoms.* 2021;498:1–8. <https://doi.org/10.1016/j.nimb.2021.04.010>.
155. Rutherford E. The scattering of  $\alpha$  and  $\beta$  particles by matter and the structure of the atom. *Philos Mag.* 1911;6:1–24.

156. L'Ecuyer J, Davies JA, Matsunami N. How accurate are absolute Rutherford backscattering yields. *Nucl Instrum Methods*. 1979;160:337–46. [https://doi.org/10.1016/0029-554X\(79\)90612-8](https://doi.org/10.1016/0029-554X(79)90612-8).
157. Andersen HH, Besenbacher F, Loftager P, Möller W. Large-angle scattering of light ions in the weakly screened Rutherford region. *Phys Rev A*. 1980;21:1891–901. <https://doi.org/10.1103/PhysRevA.21.1891>.
158. Carrasco AG, Wauters T, Petersson P et al. Nitrogen removal from plasma-facing components by ion cyclotron wall conditioning in TEXTOR. *J Nucl Mater*. 2015;463:688–92. <https://doi.org/10.1016/j.jnucmat.2014.11.113>.
159. Norbury JW, Battistoni G, Besuglow J et al. Are further cross section measurements necessary for space radiation protection or ion therapy applications? Helium projectiles. *Front Phys*. 2020;8. <https://doi.org/10.3389/fphy.2020.565954>.
160. Wolicki EA, Holmgren HD, Johnston RL, Geer Illsley E. Differential cross sections for the  ${}^9\text{Be}({}^3\text{He},\text{p}){}^{11}\text{B}$  reaction. *Phys Rev*. 1959;116:1585–91. <https://doi.org/10.1103/PhysRev.116.1585>.
161. Barradas NP, Catarino N, Mateus R et al. Determination of the  ${}^9\text{Be}({}^3\text{He},\text{p}){}^{11}\text{B}$  ( $i = 0, 1, 2, 3$ ) cross section at 135° in the energy range 1–2.5 MeV. *Nucl Instrum Methods Phys Res, Sect B, Beam Interact Mater Atoms*. 2015;346:21–5. <https://doi.org/10.1016/j.nimb.2015.01.037>.
162. Provatas G, Fazinić S, Soić N et al. Differential cross section measurements of the  ${}^9\text{Be}({}^3\text{He},\text{p}){}^{11}\text{B}$  reaction for NRA applications. *Nucl Instrum Methods Phys Res, Sect B, Beam Interact Mater Atoms*. 2020;472:36–45. <https://doi.org/10.1016/j.nimb.2020.03.039>.
163. Möller S. Analytical continuous slowing down model for nuclear reaction cross-section measurements by exploitation of stopping for projectile energy scanning and results for  ${}^{13}\text{C}({}^3\text{He},\alpha){}^{12}\text{C}$  and  ${}^{13}\text{C}({}^3\text{He},\text{p}){}^{15}\text{N}$ . *Nucl Instrum Methods Phys Res, Sect B, Beam Interact Mater Atoms*. 2017;394:134–40. <https://doi.org/10.1016/j.nimb.2017.01.017>.
164. Provatas G, Fazinić S, Soić N et al. Systematic study of the  ${}^{12}\text{C}({}^3\text{He},\text{p}){}^{14}\text{N}$  reaction for NRA applications. *Nucl Instrum Methods Phys Res, Sect B, Beam Interact Mater Atoms*. 2021;500–501:57–67. <https://doi.org/10.1016/j.nimb.2021.03.005>.
165. Krat S, Mayer M, Porosnicu C. The  ${}^9\text{Be}(\text{p},\text{p}_0){}^9\text{Be}$ ,  ${}^9\text{Be}(\text{p},\text{d}_0){}^8\text{Be}$ , and  ${}^9\text{Be}(\text{p},\alpha_0){}^6\text{Li}$  cross-sections for analytical purposes. *Nucl Instrum Methods Phys Res, Sect B, Beam Interact Mater Atoms*. 2015;358:72–81. <https://doi.org/10.1016/j.nimb.2015.05.004>.
166. Ntemou E, Kokkoris M, Lagoyannis A et al. Differential elastic scattering cross sections for deuterons on  ${}^9\text{Be}$ , at energies and angles suitable for elastic backscattering spectroscopy. *Nucl Instrum Methods Phys Res, Sect B, Beam Interact Mater Atoms*. 2019;459:90–3. <https://doi.org/10.1016/j.nimb.2019.08.032>.
167. Gurbich A, Bogdanović-Radović I, Chiari M et al. Status of the problem of nuclear cross section data for IBA. *Nucl Instrum Methods Phys Res, Sect B, Beam Interact Mater Atoms*. 2008;266:1198–202. <https://doi.org/10.1016/j.nimb.2007.11.041>.
168. Gurbich AF. SigmaCalc recent development and present status of the evaluated cross-sections for IBA. *Nucl Instrum Methods Phys Res, Sect B, Beam Interact Mater Atoms*. 2016;371:17–32. <https://doi.org/10.1016/j.nimb.2015.09.035>.

Submit your manuscript to a SpringerOpen<sup>®</sup> journal and benefit from:

- Convenient online submission
- Rigorous peer review
- Open access: articles freely available online
- High visibility within the field
- Retaining the copyright to your article

---

Submit your next manuscript at ► [springeropen.com](https://www.springeropen.com)